Study on the Preparation and Photocatalytic Performance of TiO2 Nanotube Films on the Surface of Nickel-Doped Porous Titanium

Jie Zheng , Yike Wang , TingHao Mao , Wei Feng *

Posted Date: 21 April 2026

doi: 10.20944/preprints202604.1380.v1

Keywords: Ni-doped TiO2 nanotube films; porous titanium; photocatalysis; methylene blue degradation; calcination temperature

 doi:10.20944/preprints202604.1380.v1

Article

Study on the Preparation and Photocatalytic Performance of TiO_2 Nanotube Films on the Surface of Nickel-Doped Porous Titanium

Jie Zheng [1,2], Yike Wang [1,2], TingHao Mao [1,2] and Wei Feng [1,2,*]

[1] School of Mechanical Engineering, Chengdu University, Chengdu 610106, China

[2] Sichuan Province Engineering Technology Research Center of Powder Metallurgy, Chengdu 610106, China

* Correspondence: fengwei@cdu.edu.cn

Abstract

Porous titanium materials exhibit tremendous potential in the field of photocatalytic dye degradation owing to their unique structural and performance advantages. Although traditional powder materials (such as TiO_2 nanoparticles) possess high specific surface area and active sites, they suffer from issues of difficult recovery and low light utilization efficiency. Coating materials address the recovery problem by immobilizing the catalyst; however, their limitations including limited specific surface area, insufficient visible light response, and poor mechanical stability restrict their practical applications. In contrast, bulk materials with in-situ grown nano-sized titanium dioxide on the surface of a titanium core combine high specific surface area, enhanced visible light absorption capacity, and excellent mechanical stability, making them an ideal choice for photocatalytic dye degradation. In this study, nickel-doped porous titanium was used as the substrate, and Nix-TiO_2 nanotube films with a three-dimensional (3D) network structure were successfully prepared via an in-situ hydrothermal method. The effects of nickel content (2.5 wt.%, 5 wt.%, 7.5 wt.%, 10 wt.%) and calcination temperature (350 ℃-750 ℃) on the structure, morphology, and photocatalytic performance of the composite materials were systematically investigated. X-ray diffraction (XRD), scanning electron microscopy (SEM), X-ray photoelectron spectroscopy (XPS), and nitrogen adsorption-desorption (BET) techniques were employed to characterize the phase composition, micromorphology, chemical state, and specific surface area of the samples. Methylene blue (MB, 20 mg/L) was selected as the target pollutant to evaluate the photocatalytic activity and stability of the catalysts under simulated sunlight. Results indicated that nickel did not enter the TiO_2 lattice but formed nickel oxide (NiO), constructing a semiconductor composite structure. Among all samples, the Ni7.5-TiO_2 catalyst exhibited the optimal photocatalytic performance, achieving a 98.35% MB degradation rate within 3 hours and maintaining excellent cyclic stability after 5 consecutive degradation cycles. The optimal calcination temperature was determined to be 450 ℃, at which TiO_2 nanotubes were completely in the anatase phase with an intact 3D network structure and high crystallinity. Compared with pure titanium substrates, the porous titanium-based catalyst showed a significant enhancement in adsorption capacity, and nickel doping further improved this performance by increasing the specific surface area and providing more active sites. The synergistic effect of nickel doping and the porous titanium-based nanotube structure effectively narrowed the TiO_2 band gap, inhibited the recombination of photogenerated carriers, and improved solar energy utilization efficiency. This study provides a feasible technical approach for the treatment of wastewater containing organic pollutants and enriches the research on modified TiO_2 photocatalytic materials.

Keywords: Ni-doped TiO_2 nanotube films; porous titanium; photocatalysis; methylene blue degradation; calcination temperature

 doi:10.20944/preprints202604.1380.v1

1. Introduction

With the advancement of urbanization and industrialization, environmental pollution is increasing day by day. In the process of sewage discharge, industrial wastewater usually needs to be treated; however, pollutants in industrial wastewater continue to affect our environment due to their complex molecular structure, stability, and refractory characteristics. As a traditional photocatalytic material, TiO_2, when irradiated by ultraviolet (UV) light with a wavelength less than 387 nm, undergoes valence band electron transition to the conduction band, forming photogenerated electron-hole pairs. The holes react with surface-adsorbed water to generate hydroxyl radicals, while the electrons combine with oxygen to form superoxide radicals[1]. These two highly oxidizing species can decompose over 90% of common organic pollutants.

TiO_2 has a wide band gap, which allows it to absorb only UV light with a wavelength below 400 nm, limiting its activity to the UV region[2]. In addition to the wide band gap, photogenerated electron-hole pairs are prone to recombination. However, nickel doping can precisely solve these two key issues, while synergizing with the porous titanium-based nanotube structure to achieve a performance leap. Nickel doping can narrow the band gap of TiO_2: Ni^{2+}, as an impurity atom, introduces new impurity energy levels in the band gap of TiO_2, reducing the energy required for photogenerated electron transition[2]. This expands the material's applicable range from the UV region to the visible light region, significantly improving the solar energy capture efficiency. Nickel doping can inhibit the recombination of photogenerated carriers: Ni^{2+} can act as a "carrier trapping center" to selectively capture photogenerated electrons on the TiO_2 surface, preventing rapid combination of electrons and holes[2]. Meanwhile, the energy level difference between Ni^{2+} and TiO_2 can guide carriers to migrate to the material surface, enabling more active carriers to participate in catalytic reactions such as pollutant degradation and water splitting, directly improving the reaction efficiency[2].

Therefore, in this work, nickel-doped porous titanium was used as the substrate, and Ni_x-TiO_2 nanotubes were in-situ prepared on its surface via a hydrothermal method. Composite catalysts with different compositions were obtained by controlling the mass fraction of nickel powder. The effects of nickel content on the photocatalytic activity of the catalyst for methylene blue (MB) degradation and the stability of the catalyst were investigated. The influence of calcination temperature on its crystal phase was explored, and its structure, morphology, and optical properties were characterized. Finally, the photocatalytic reaction mechanism was proposed.

2. Experiments

2.1. Preparation of Porous Titanium Doped with Different Nickel Contents

First, irregular pure titanium powder (purity > 99.5%, particle size < 50 μm) and nickel powder (purity > 99.5%, particle size < 50 μm) were weighed in a certain proportion. The mass fractions of nickel in this experiment were 2.5 wt.%, 5 wt.%, 7.5 wt.% and 10 wt.%. Subsequently, the weighed titanium powder and nickel powder were placed into a omnidirectional planetary ball mill PM-QW4 for uniform mixing. The ball milling parameters were as follows: stainless steel balls were used as the milling medium, with a ball-to-powder ratio of 10:1 and a milling speed of 150 r/min. The program was set to "mill for 0.5 h and stop for 0.5 h, with a forward-reverse rotation switching frequency of once per hour", and the total milling time was 6 h. Since titanium is a highly active and easily oxidizable metal material, the stainless steel milling jar was filled with high-purity argon before the start of ball milling.

After obtaining the uniformly mixed titanium-nickel powder, spark plasma sintering (SPS) was adopted[2]. Then, the mixed powder was blended with 60 wt.% NaCl (used as a pore-forming agent) in proportion to prepare porous titanium with a unique pore structure. Next, the mixed powder was loaded into a graphite mold and placed into a spark plasma sintering apparatus for sintering. The sintering parameters were set as follows: the pressure was 30 MPa, the sintering temperature was 600 ℃, and the heating rate was controlled at 100 ℃ per minute. When the temperature reached the

 doi:10.20944/preprints202604.1380.v1

specified value, it was held for 10 minutes, followed by furnace cooling, and finally the sample was obtained.

2.2. Preparation of TiO_2 Nanotube Thin Films

First, the samples were subjected to pretreatment. After sintering, the graphite paper adhering to the sintered billet was removed with sandpaper, and the surface of the sintered billet was polished to a depth of 1 mm to 2 mm. Subsequently, the billet was placed in a beaker filled with water, and the beaker was put into an oven at 80℃ for 2 hours to allow the moisture in the sample to evaporate thoroughly[2]. Then, the mass of the sample was measured, and the above operation was repeated several times to remove the sodium chloride (NaCl), finally obtaining the porous titanium sample[2].

After pretreatment, a hydrothermal method was used to prepare a three-dimensional (3D) networked TiO_2 nanotube film on the surface of porous titanium. 10 mol/L sodium hydroxide (NaOH) aqueous solution and the nickel-doped porous titanium sheet were placed into a polytetrafluoroethylene (PTFE)-lined autoclave[2]. The autoclave was then sealed and heated in an oven at 180 ℃ for 8 hours. After hydrothermal treatment, the sample was taken out and washed repeatedly with deionized water until its pH reached approximately 7. Afterwards, the sample was immersed in 0.1 M hydrochloric acid (HCl) aqueous solution for 12 hours, and then rinsed with deionized water until the pH was around 7. The washed sample was then placed in a drying oven for drying. Finally, the dried sample was calcined at 450 ℃ for 2 hours, with the heating and cooling rates controlled at 2 ℃/min.

2.3. Investigation on the Effect of Heat Treatment Temperature on the Crystal Structure and Photocatalytic Performance of Catalysts

Both the crystal phase structure and crystallinity of titanium dioxide (TiO_2) have a significant impact on its photocatalytic performance, while calcination temperature is regarded as a key factor affecting the phase structure, crystallinity, grain size, and specific surface area[2]. Therefore, to investigate the effect of calcination temperature on the prepared catalyst, $Ni_{7.5}$-TiO_2—the catalyst with the best photocatalytic performance—was selected as the sample. It was calcined at 350 ℃, 450 ℃, 550 ℃, 650 ℃, and 750 ℃ respectively, followed by characterization and performance analysis.

2.4. Characterization of Materials

X-ray diffraction (XRD) technology[2], as one of the important methods for studying the structure of polycrystalline materials, is widely used in the structural characterization of various compounds and their derivatives. In this study, a DX-2700B X-ray diffractometer was used to analyze the phase composition of the prepared porous material samples, samples during the hydrothermal process, and samples after calcination. The XRD test conditions were as follows: monochromatic Cu Kα radiation (λ=1.541 Å) was adopted, with a scanning range of 20°–90°, a step scanning angle of 0.02°, an operating voltage of 40 kV, an operating current of 40 mA, and a sampling time interval of 0.5 s.

Scanning electron microscopy (SEM) can effectively display surface information such as the micromorphology and particle size of materials, with a large depth of field and a wide range of magnification[2]. In this experiment, a ZEISS Sigma 300 was used to characterize and analyze the micromorphologies of raw titanium powder, titanium powder morphology in bulk samples, pore structure, and nanotubes[2].

In this study, methylene blue (MB) with a concentration of 20 mg/L was used as the pollutant model to evaluate the photocatalytic performance of the photocatalysts. A CEL-S500 500W xenon lamp was used as the light source. First, 50 mL of MB solution was placed in the reaction device, and the porous titanium sample was placed at the bottom of the device. Before irradiation, the MB solution containing the porous titanium sample was stirred in the dark for 1 hour to reach adsorption equilibrium[2]. Then, it was placed under the xenon lamp for photocatalytic reaction, with the distance between the porous titanium sample and the light source maintained at 15 cm, and the irradiation

 doi:10.20944/preprints202604.1380.v1

time was 3 hours. During the experiment, the solution was sampled every 30 minutes, and its absorbance was measured using an ultraviolet-visible (UV-Vis) spectrophotometer with a test wavelength range of 500 nm–750 nm. Subsequently, the degradation rate was calculated using the formula. The formula for calculating the degradation rate P is[2]:

$$P=(C_0-C_t)/C_0\times100\% \quad (2.1)$$

Among them, P is the degradation rate; C_0 is the initial concentration of the solution; C_t is the concentration of the solution at time t.

To analyze the effect of Ni content on the phase composition of TiO_2 nanotubes, a series of prepared materials were characterized by X-ray diffraction (XRD). The morphology of Ni-doped samples was observed using a scanning electron microscope (SEM), and nitrogen adsorption-desorption tests were employed to investigate the pore size distribution and specific surface area of the photocatalysts doped with different Ni contents[2].

3. Results

3.1. Characterization and Analysis of Titanium Dioxide Nanotubes on Porous Titanium with Different Nickel Contents

3.1.1. XRD Analysis

To analyze the effect of Ni content on the phase of TiO_2 nanotubes, a series of prepared materials were characterized by XRD, and the results are shown in Figure 3.1. It can be observed from the figure that all samples exhibit sharp and distinct diffraction peaks at 2θ = 25.3°, 37.9°, 48.15°, 54.05°, 55.2°, 62.8°, and 75.27°. By comparing with the standard diffraction pattern (PDF No. 78-2486), these peaks are identified as the characteristic peaks of anatase TiO_2, corresponding to the (101), (004), (200), (105), (211), (204), and (215) crystal planes, respectively.When the Ni doping content is 0 wt.%, in addition to the diffraction peaks of anatase TiO_2, diffraction peaks of Ti are also present at 2θ = 35.09°, 38.42°, 40.17°, 53°, 70.66°, 72.21°, and 77.36°. With the addition of Ni, new diffraction peaks appear at 2θ = 37.24°, 43.27°, 44.49°, and 51.84°. According to the standard diffraction pattern (PDF No. 87-0712), the peaks at 2θ = 44.49° and 51.84° are attributed to Ni. The peaks at 2θ = 37.24° and 43.27° correspond to the standard diffraction pattern of NiO (PDF No. 47-1049), while the (220) peak of NiO at 62.8° overlaps with that of anatase TiO2[2].This indicates that after hydrothermal treatment and calcination of the Ni-doped porous titanium substrate, Ni does not enter the lattice of TiO_2 but forms NiO, which is a typical composite of two semiconductors[2].

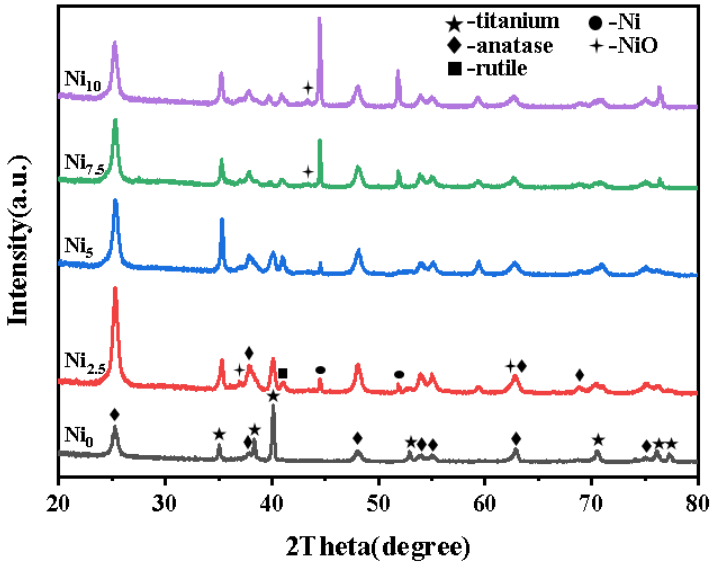

Figure 3.1. XRD patterns of samples with different nickel contents.

 doi:10.20944/preprints202604.1380.v1

3.1.2. SEM Analysis

The morphologies of the samples after Ni doping are shown in Figure 3.2. It can be observed from the figure that the surfaces of the catalysts prepared with different Ni contents (2.5 wt.%, 5 wt.%, 7.5 wt.%, 10 wt.%) are completely covered by interconnected nanotube networks. The nanotubes cross each other to form numerous pores with diameters less than 100 nm[2]. This structure is beneficial for incident light absorption, as the incident light can scatter inside the networked nanotube film, thereby improving the incident light absorption rate[2]. When comparing the catalysts prepared with different Ni contents, there is no significant difference in their surface morphologies, indicating that the catalyst has a relatively stable crystal structure and high reusability.

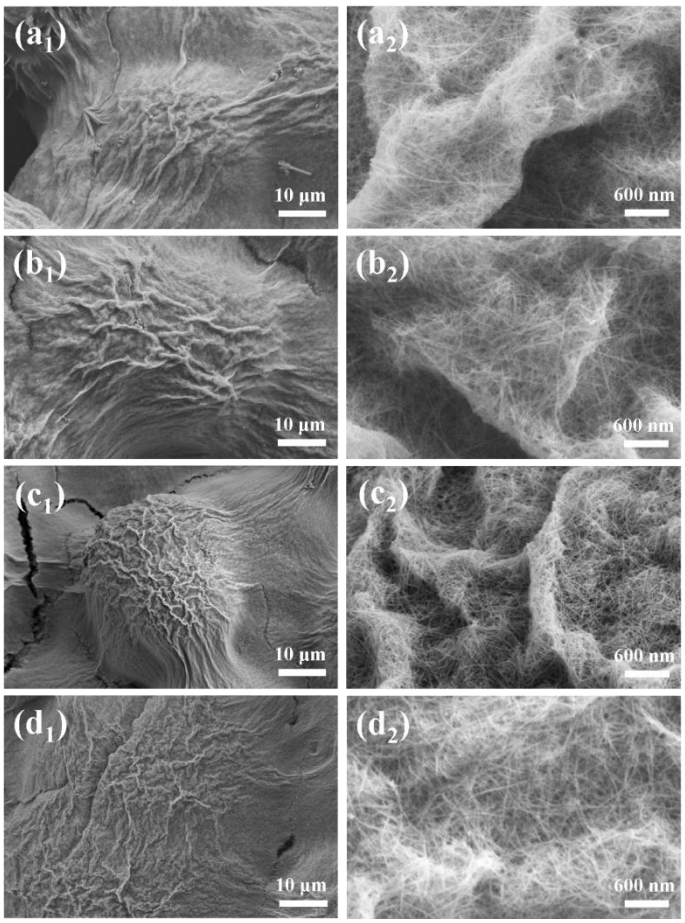

Figure 3.2. SEM images of samples with different nickel contents (a) $Ni_{2.5}$-TiO_2; (b) Ni_5-TiO_2; (c) $Ni_{7.5}$-TiO_2; (d) Ni_{10}-TiO_2.

3.1.3. XPS Analysis

Figure 3.3 shows the X-ray photoelectron spectroscopy (XPS) spectra of the $Ni_{7.5}$-TiO_2 nanotube networks. Compared with the XPS spectra of undoped Ni samples in Chapter 3, there is no significant difference in the XPS spectra of O 1s and Ti 2p. From the O 1s XPS spectrum, it can be observed that the main existing form of oxygen in the catalyst is still TiO_2. The peak at the binding energy of 529.8 eV corresponds to the Ti-O bond, i.e., the binding energy of lattice oxygen, while the shoulder peak at 531.54 eV is related to surface hydroxyl groups. Compared with the XPS spectrum of undoped Ni, the O 1s peak of $Ni_{7.5}$-TiO_2 shows a slight shift toward the higher binding energy direction, which may be attributed to the introduction of Ni element. In the Ti 2p spectrum, two main peaks are observed at 464.2 eV and 458.5 eV, corresponding to Ti^{4+} (TiO_2) 2p1/2 and Ti^{4+} (TiO_2) 2p3/2, respectively. The energy difference of 5.7 eV between the two peaks indicates that Ti element mainly exists in the form of Ti^{4+}. Meanwhile, a shoulder peak at 457.7 eV corresponds to the binding energy

 doi:10.20944/preprints202604.1380.v1

of Ti^{3+}.Figure 3.3 confirms that the TiO_2 nanotube networks contain Ni element, which is consistent with the EDS data. Several impurity peaks appear in the spectrum due to the low content of Ni and weak signal. The peaks at binding energies of 855.6 eV and 873.3 eV correspond to Ni 2p3/2 and Ni 2p2/1, respectively, indicating that Ni element mainly exists in the +2 valence state[2].

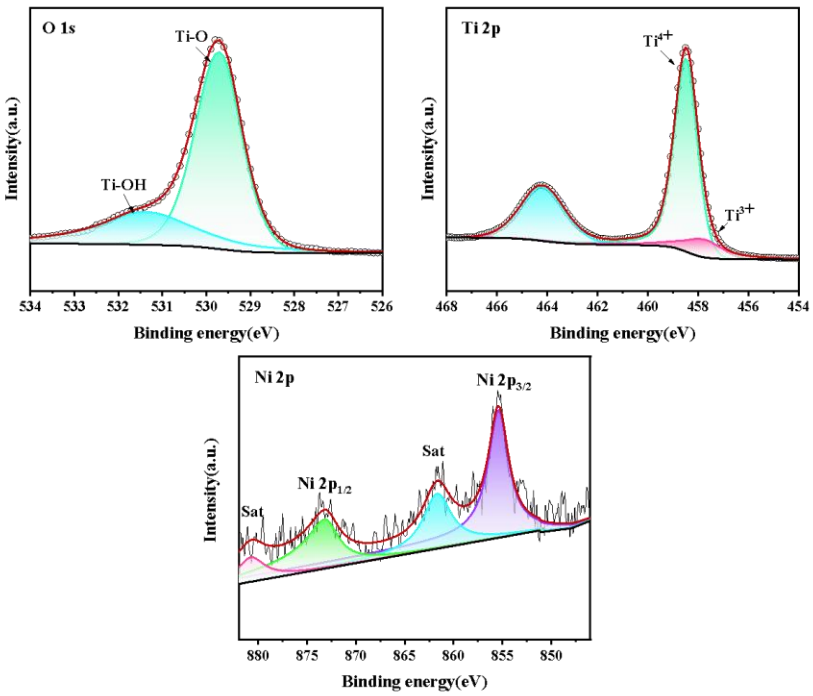

Figure 3.3. XPS image of $Ni_{7.5}$-TiO_2 nanotubes: (a) O 1s; (b) Ti 2p; (c) Ni 2p.

3.1.4. BET Analysis

N_2 adsorption-desorption measurements were conducted to investigate the pore size distribution and specific surface area of photocatalysts doped with different Ni contents[2], and the results are shown in Figure 3.4. From the N_2 adsorption-desorption isotherms of the materials, it can be seen that within the relative pressure (P/P0) range of 0.0–1.0, the isotherms of the samples are type IV with distinct H3 hysteresis loops, indicating that the photocatalysts have a mesoporous structure. This may be attributed to the numerous pore structures of porous titanium and the micropores existing between the interconnected TiO_2 nanotubes, which is consistent with the SEM results.Compared with the undoped sample, the specific surface areas of Ni_x-TiO_2 are all improved to a certain extent[2]. The specific surface areas of $Ni_{2.5}$-TiO_2, Ni_5-TiO_2, $Ni_{7.5}$-TiO_2, and Ni_{10}-TiO_2 are 24.36 m^2/g, 26.78 m^2/g, 31.87 m^2/g, and 26.3 m^2/g, respectively. The results show that Ni doping can effectively improve the specific surface area of TiO_2, which may be because the doping of a small amount of Ni can inhibit the growth of TiO_2 lattice, leading to an increase in the specific surface area of the photocatalyst. Figure 3.4(b) shows the pore size distribution of the prepared samples[2]. It can be observed from the figure that the pore size distribution of the catalysts is mainly below 50 nm, further confirming that the materials have a mesoporous structure[2].

 doi:10.20944/preprints202604.1380.v1

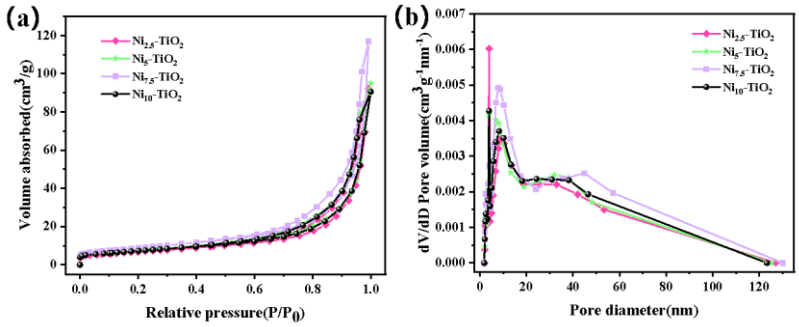

Figure 3.4. (a) N2 adsorption-desorption isotherms and (b) pore size distributions for samples.

3.1.5. Study on the Performance of Photocatalytic Degradation of Dyes

To investigate the catalytic activity of the prepared nickel-doped photocatalyst under visible light, methylene blue (MB) solution with a concentration of 20 mg/L was used as the degradation substrate. First, the reaction was conducted at a hydrothermal temperature of 200 ℃ for a hydrothermal duration of 2 h[2]. After the reaction, the product was subjected to acid washing with 0.1 M hydrochloric acid (HCl) for 12 h; subsequent to drying, it was annealed in a muffle furnace at 450 ℃ for 2 h. Once cooled, the porous titanium sample was placed at the bottom of the reaction vessel, and 50 mL of the methylene blue solution was added to the reaction device for photocatalytic degradation. Prior to light irradiation, the methylene blue solution containing the porous titanium sample was stirred in the dark for 1 h to achieve adsorption equilibrium, followed by a 3-hour visible light irradiation period for the photocatalytic reaction.Figure 3.5 shows the photocatalytic performance of TiO_2 nanotube array catalysts prepared with different nickel doping amounts. Figure 3.5a presents the absorbance spectrum of methylene blue solution with $Ni_{7.5}/TiO_2$ catalyst as a function of irradiation time. The results indicate that the peak intensity of absorbance of the methylene blue solution containing the catalyst gradually decreases with the increase of irradiation time. The absorbance of the methylene blue solution gradually decreases to nearly zero, meaning that the methylene blue dye is almost completely removed[2]. Figure 3.5b intuitively displays the degradation of methylene blue by $Ni_{2.5}$-TiO_2, Ni_5-TiO_2, $Ni_{7.5}$-TiO_2, and Ni_{10}-TiO_2 within 3 hours. All four catalysts exhibit excellent degradation effects on methylene blue under simulated sunlight, with degradation rates all above 90%[2]. Among them, $Ni_{7.5}$-TiO_2 shows the best degradation performance, degrading 85.33% of methylene blue within 90 minutes and achieving the highest degradation rate of 98.35% at 180 minutes, almost completely degrading methylene blue. As shown in Figure 3.5c, the degradation reactions of methylene blue by the four catalysts all conform to the first-order kinetics, with correlation coefficients all above 98%. From the first-order kinetic curves, it can be obtained that $Ni_{7.5}$-TiO_2 has the highest rate constant of 0.02368 min^{-1}, which is 1.56 times, 1.31 times, and 1.42 times that of Ni2.5-TiO2 (0.01515 min^{-1}), Ni_5-TiO_2 (0.01812 min^{-1}), and Ni_{10}-TiO_2 (0.01666 min^{-1}), respectively[2]. Figure 3.5d is a line chart of the degradation rates of methylene blue by the four catalysts after 3 hours of irradiation under simulated sunlight. It can be intuitively seen from the figure that $Ni_{7.5}$-TiO_2 has the best degradation effect on methylene blue, reaching 98.35%, while the degradation rates of $Ni_{2.5}$-TiO_2, Ni_5-TiO_2, and Ni_{10}-TiO_2 are 92.8%, 96.11%, and 94.99%, respectively.

 doi:10.20944/preprints202604.1380.v1

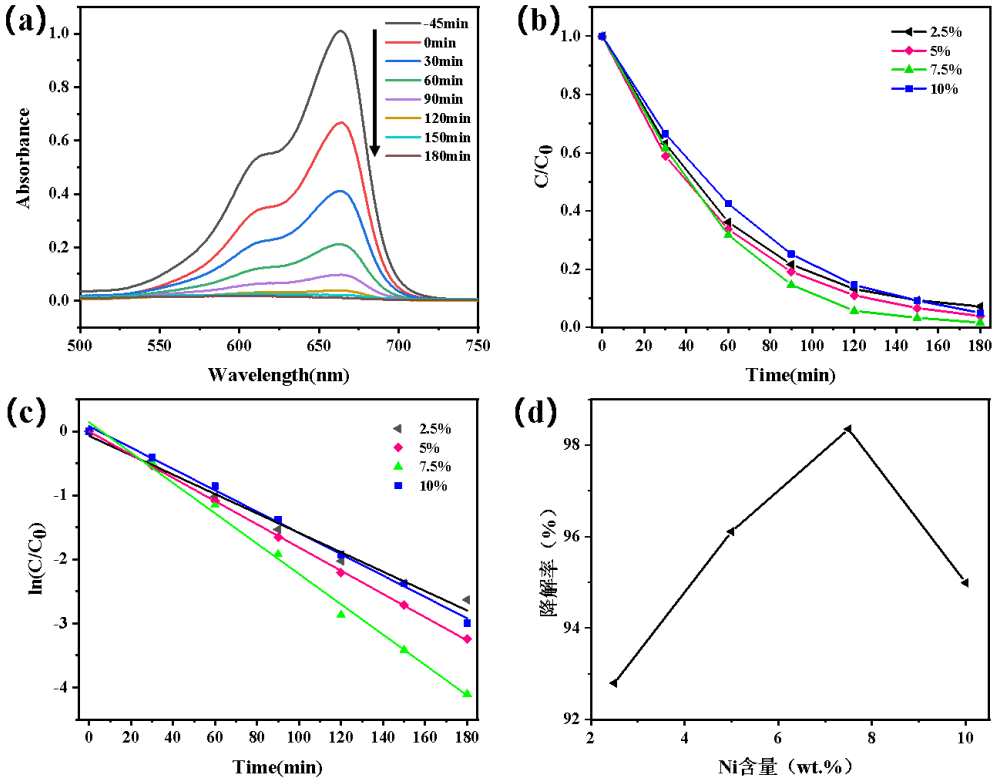

Figure 3.5. Photocatalytic activity of samples to degrade MB (a) Absorbance change curve of $Ni_{7.5}/TiO_2$ degraded MB; (b) Photocatalytic activity of four catalysts for MB degradation; (c) The corresponding first-order kinetic curves; (d) Line graph of degradation rate of MB at 3h with four catalysts.

3.1.6. Adsorption Performance of Photocatalysts

Experiments revealed a significant change in the absorbance of the solution following dark treatment. Accordingly, photocatalysts based on pure titanium sheets and porous titanium doped with varying nickel mass fractions were selected as samples, and the concentration of methylene blue solution after dark treatment was determined[2]. The results are presented in Figure 3.6. As indicated in the figure, the photocatalyst with pure titanium sheet as the substrate shows the weakest adsorption capacity, whereas all samples using porous titanium as the substrate exhibit excellent adsorption performance[2]. This is attributed to the high porosity of porous titanium, which endows it with a larger specific surface area compared to pure titanium sheets. During dark treatment, materials with a high specific surface area can adsorb more molecules, thereby enhancing the adsorption efficiency. In addition, due to the diverse pore structures of porous titanium substrates[2], the mesoporous structure is favorable for catalyst loading. Medium-sized mesopores not only ensure a high specific surface area but also reduce mass transfer resistance. In contrast, the macroporous structure is more suitable as a catalyst carrier for macromolecules, since its larger pore size allows macromolecules to enter and diffuse easily, thus improving the efficiency of adsorption and catalytic reactions[2]. Furthermore, it can be observed from the figure that nickel doping slightly enhances the adsorption performance, with $Ni_{7.5}$-TiO_2 demonstrating the optimal adsorption capacity.

 doi:10.20944/preprints202604.1380.v1

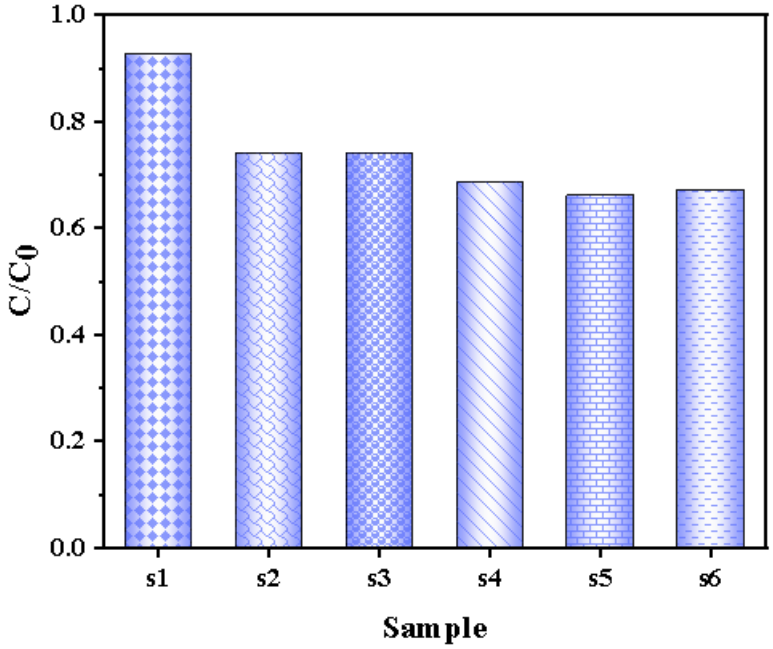

Figure 3.6. Adsorption performance experiments of catalysts: (s1) Pure titanium sheet; (s2) Ni_0-TiO_2; (s3) $Ni_{2.5}$-TiO_2; (s4) Ni_5-TiO_2; (s5) $Ni_{7.5}$-TiO_2; (s6) Ni_{10}-TiO_2.

3.2. Effect of Heat Treatment Temperature on the Crystal Phase and Photocatalytic Performance of Catalysts

3.2.1. XRD Analysis

Figure 3.7 presents the XRD patterns of Ni_x-TiO_2 nanotube arrays fabricated at different calcination temperatures. As can be seen from the figure, after calcination at 350 ℃, distinct characteristic diffraction peaks emerge at 2θ = 25.3° and 2θ = 48.1°, corresponding to the (101) and (200) crystal planes of the anatase phase of TiO_2. The diffraction peaks at 2θ = 44.49° and 2θ = 51.84° are attributed to nickel (Ni). When the heat treatment temperature is increased to 450 ℃, TiO_2 remains entirely composed of the anatase phase; meanwhile, the diffraction peak intensity of the (101) crystal plane is significantly enhanced, indicating improved crystallinity[2]. In addition, the diffraction peaks at 2θ = 37.24° and 2θ = 43.27° match the standard XRD pattern of NiO (PDF No. 47-1049), confirming the formation of NiO.

 doi:10.20944/preprints202604.1380.v1

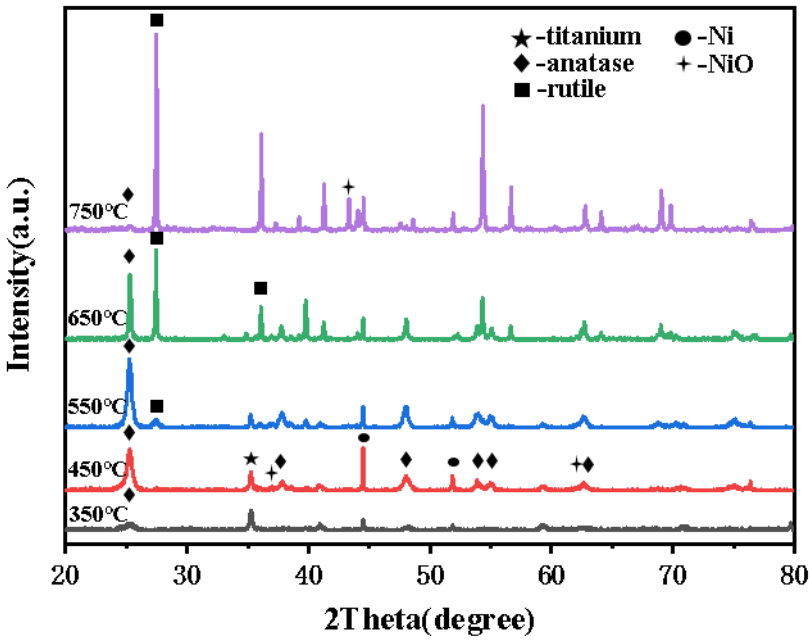

Figure 3.7. XRD patterns of samples with different heat treatment temperatures.

Furthermore, the diffraction peaks of the titanium substrate and Ni are still relatively intense at this temperature. When the heat treatment temperature is further elevated to 550 ℃, the intensity of the anatase diffraction peak corresponding to the (101) crystal plane is further strengthened, demonstrating enhanced crystallinity[2]. Simultaneously, a new weak diffraction peak is detected at 2θ = 27.4°, which corresponds to the (110) crystal plane of the rutile phase. However, the weak intensity of this diffraction peak indicates that although the rutile phase transformation temperature is reached, only a small portion of larger anatase grains are preferentially converted into the rutile phase. At this point, the two phases coexist, forming a mixed crystal phase of anatase and rutile[2]. It is generally accepted that the photocatalytic performance of anatase-phase TiO_2 is superior to that of rutile-phase TiO_2. Nevertheless, studies have shown that anatase and rutile phases can exert a synergistic effect when present in an appropriate proportion[2]. Owing to the difference in Fermi levels between the two TiO_2 polymorphs, a Schottky barrier is formed at the phase interface, which facilitates the transfer and separation of electrons and holes between the phases as well as their migration to the catalyst surface. Meanwhile, due to the intimate contact between the two phases, electrons transfer from the rutile phase to the anatase phase, reducing the electron-hole recombination rate and thus enhancing the photocatalytic activity of the material[2]. However, in this study, as observed in Figure 3.7, the TiO_2 nanotubes exhibit slight damage at 550 ℃. According to the photocatalytic results, the degradation efficiency of the sample at a heat treatment temperature of 550 ℃ is slightly lower than that at 450 ℃, indicating that the factors affecting the photocatalytic activity of the sample are multifaceted, and judgments should be made based on practical conditions. When the heat treatment temperature rises to 650 ℃, the diffraction peak of the TiO_2 rutile phase corresponding to 2θ = 27.4° is significantly enhanced and surpasses that of the anatase phase, indicating increased crystallinity of the rutile phase[2]. When the heat treatment temperature reaches 750 ℃, the intensity of the rutile phase diffraction peak (110) increases sharply, while the intensity of the anatase characteristic diffraction peak corresponding to the (101) crystal plane decreases significantly, indicating that most of the anatase phase has transformed into the rutile phase at this temperature.

In summary, at a calcination temperature of 450 ℃, the TiO_2 nanotubes are entirely composed of the anatase phase. When the temperature reaches 550 ℃, a small amount of anatase transforms

 doi:10.20944/preprints202604.1380.v1

into rutile, leading to the formation of a mixed anatase-rutile phase in the TiO_2 nanotubes. With the further increase of calcination temperature, the proportion of anatase transforming into rutile increases[2]. At 750 ℃, the TiO_2 nanotubes consist predominantly of the rutile phase. Besides the above phenomena, characteristic peaks corresponding to Ni and NiO are observed in all samples under different calcination temperatures.

The content of crystal phases in samples obtained at different heat treatment temperatures can be calculated according to Formula 3.1:

$$\chi = \frac{1}{1+0.8\frac{I_A}{I_R}} \tag{3.1}$$

where χ is the mass fraction of the rutile phase; IA is the diffraction peak intensity of the anatase phase (101); and IR is the diffraction peak intensity of the rutile phase (110). In addition, the grain size of TiO_2 nanotubes can be calculated using the Scherrer equation, which is expressed as follows:

$$D = \frac{K\lambda}{B\cos\theta} \tag{3.2}$$

Among them, D represents the average grain size; K is a constant, usually taken as 0.89; B is the full width at half maximum of the diffraction peak; λ is the wavelength of the characteristic X-ray. A Cu target was used in this experiment, so λ is 0.154056 nm. The calculated results of the relative contents of anatase and rutile phases, as well as the average grain size of TiO_2 nanotubes prepared at different heat treatment temperatures, are shown in the following table[2]:

Table 3. Effect of heat treatment temperature on phase composition and grain size of TiO_2.

calcination temperature (℃)	average grain size (nm)		mass fraction (%)	
	anatase (101)	Rutile (110)	anatase	Rutile
350	9.1	——	100	——
450	14.05	——	100	——
550	17.4	16.8	81.7	18.3
650	44.15	65.4	40.1	59.9
750	27.7	85.5	4.9	95.1

As shown in Table 3.1, with the increase of heat treatment temperature, the average grain sizes of both the anatase phase and rutile phase increase correspondingly[2]. This is because the crystallinity of titanium dioxide (TiO_2) gradually improves as the heat treatment temperature rises. At lower temperatures, TiO_2 may be in an amorphous state or a state with low crystallinity, and the grain size is small at this time. When the temperature increases, the amorphous structure gradually transforms into a crystalline structure, leading to an increase in grain size. In addition, the anatase phase will gradually transform into the rutile phase at higher temperatures[2]. During this process, grains continue to grow by absorbing surrounding atoms or small grains. Compared with the anatase phase, the rutile phase has higher thermal stability, so it is easier to form larger-sized grains at high temperatures.

3.2.2. SEM Analysis

Figure 3.8 shows the SEM images of $Ni_{7.5}$-TiO_2 nanotubes treated at different calcination temperatures. As can be seen from the images, a uniform thin film is grown on the surface of porous titanium, with distinct differences in micromorphology under varying calcination temperatures. No obvious differences are observed between the samples calcined at 350 ℃ and 450 ℃, both of which exhibit intact nanotubular structures with uniform sizes. When the temperature reaches 550 ℃, a small amount of nanoparticles can be observed (see Figure 3.8c), indicating that the nanotubes are damaged—they split into multiple segments, resulting in shortened tube lengths. However, when the temperature exceeds 550 ℃, the morphology changes significantly. As shown in Figure 3.8d, most nanotubes collapse and gradually transform into nanoparticles with diameters ranging from 50 nm to 100 nm. This is because calcination induces microcracks in the nanotube film, leading to its

 doi:10.20944/preprints202604.1380.v1

detachment. When the temperature is further increased to 750 ℃, the nanotubes are completely fractured, forming nanoparticles with diameters larger than 100 nm. It can be concluded that a higher temperature provides more energy to dissolve the nanotubes[2]. Combined with the XRD results , it is found that $Ni_{7.5}$-TiO_2 nanotubes undergo a phase transformation from anatase to rutile during the calcination process. This phase transformation may cause volume changes, which in turn may result in the breakage of the nanotubes. In particular, when the calcination temperature exceeds 550 ℃, the transformation from anatase to rutile becomes more pronounced[2]. This transformation is accompanied by volume expansion, which is likely to cause the destruction of the nanotube structure. Therefore, intact nanotubes can be obtained by maintaining the calcination temperature at 450 ℃.

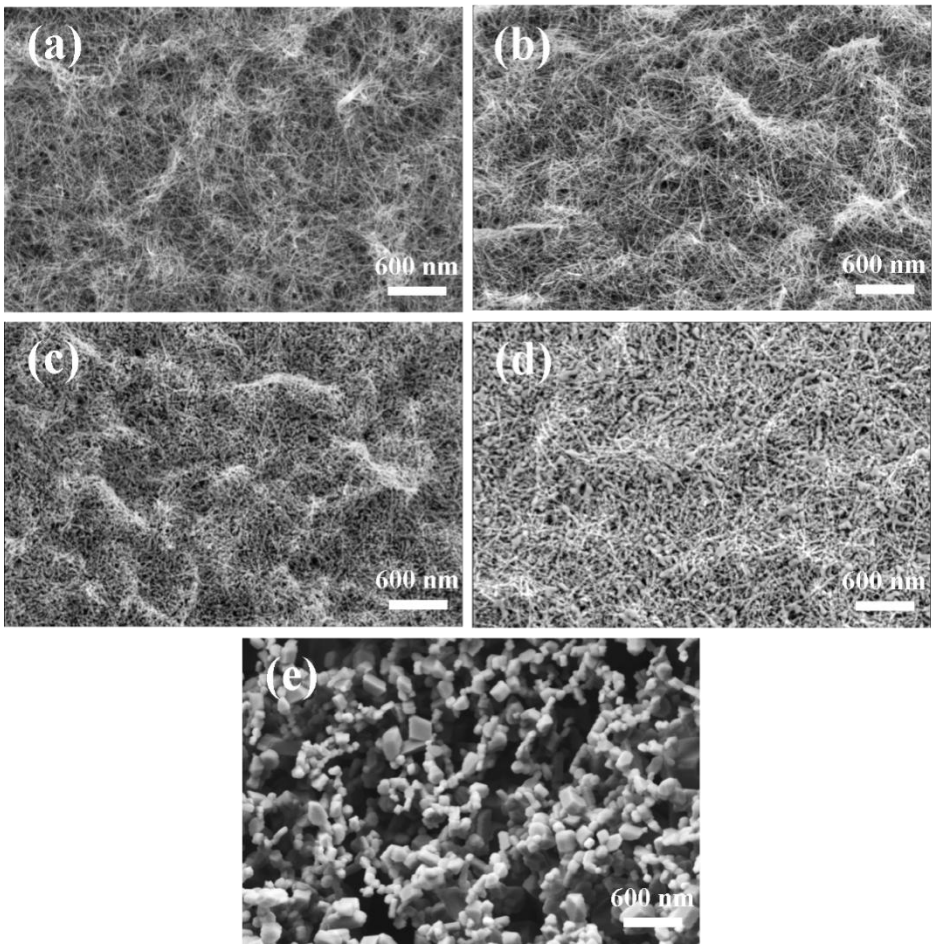

Figure 3.8. SEM of $Ni_{7.5}$-TiO_2 nanotubes prepared by different heat treatment conditions (a) 350℃; (b) 450℃; (c) 550; (d) 650℃; (e) 750℃.

3.2.3. Study on Photocatalytic Degradation Performance of Dyes

Figure 3.9 shows the MB degradation efficiency of $Ni_{7.5}$-TiO_2 nanotubes within 3 hours under different calcination conditions. As presented in Figure 3.9a, the sample calcined at 350 ℃ exhibits relatively low photocatalytic activity, with MB degradation rates of 84.886% and 91.916% within 2 hours and 3 hours, respectively. Combined with the analysis of Figure 3.7, this is presumably attributed to the low crystallinity of anatase TiO_2[2]. With the increase of calcination temperature, the photocatalytic activity of the samples increases and reaches the maximum at 450 ℃. The sample calcined at 450 ℃ achieves MB degradation rates of 94.311% (2 h) and 98.353% (3 h). Based on the XRD and SEM results, the sample treated at 450 ℃ possesses high crystallinity, along with well-defined and intact nanotube structures; thus, 450 ℃ is determined as the optimal calcination temperature. As the calcination temperature continues to rise, the photocatalytic activity gradually decreases, hitting the lowest at 750 ℃—with MB degradation rates of 80.828% (2 h) and 92.899% (3

 doi:10.20944/preprints202604.1380.v1

h) for the sample treated at this temperature. The reduced photocatalytic activity of samples calcined above 450 ℃ may result from the following factors. First, according to the XRD results, a phase transformation from anatase to rutile occurs in the temperature range of 550 ℃ to 750 ℃. Compared with the anatase phase, the rutile phase exhibits lower photocatalytic activity. Second, as indicated by the SEM results, the nanotube structure gradually deteriorates with increasing temperature, leading to a corresponding decrease in specific surface area, which further reduces the photocatalytic activity[2]. Figure 3.9b demonstrates that all samples fit the first-order kinetic curve. Through calculation, the rate constants (K values) of the samples under different calcination temperatures are obtained, among which the sample calcined at 450 ℃ has the highest rate constant of 0.02368 min-1.

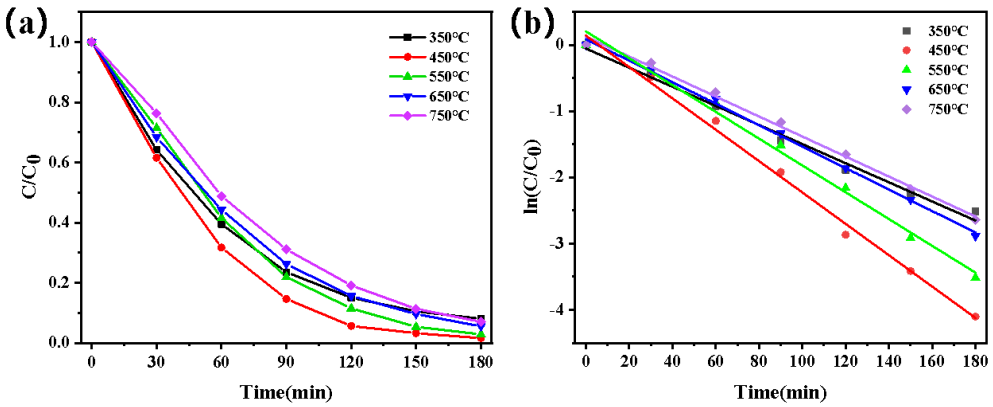

Figure 3.9. Degradation rates and fitting curves of methylene blue in specimens with different heat treatment conditions.

3.2.4. Adsorption Performance of Photocatalysts

Figure 3.10 shows the adsorption performance of each catalyst toward dye molecules after calcination at different temperatures. As can be seen from the figure, the catalyst exhibits the maximum adsorption performance at a calcination temperature of 350 ℃. With the increase of calcination temperature, the adsorption performance decreases gradually[2]. This phenomenon is attributed to the damage of the nanotube structure caused by elevated temperatures—when the calcination temperature reaches 750 ℃, the nanotubes have been transformed into nanoparticles with diameters larger than 100 nm. Consequently, the specific surface area of the catalyst is reduced. A smaller specific surface area implies a decreased contact area between the catalyst and reactants, thereby lowering the adsorption capacity for reactants. Additionally, the reduced specific surface area may result in a decrease in the number of pores or a shrinkage of pore size, which in turn hinders the mass transfer of reactants[2].

 doi:10.20944/preprints202604.1380.v1

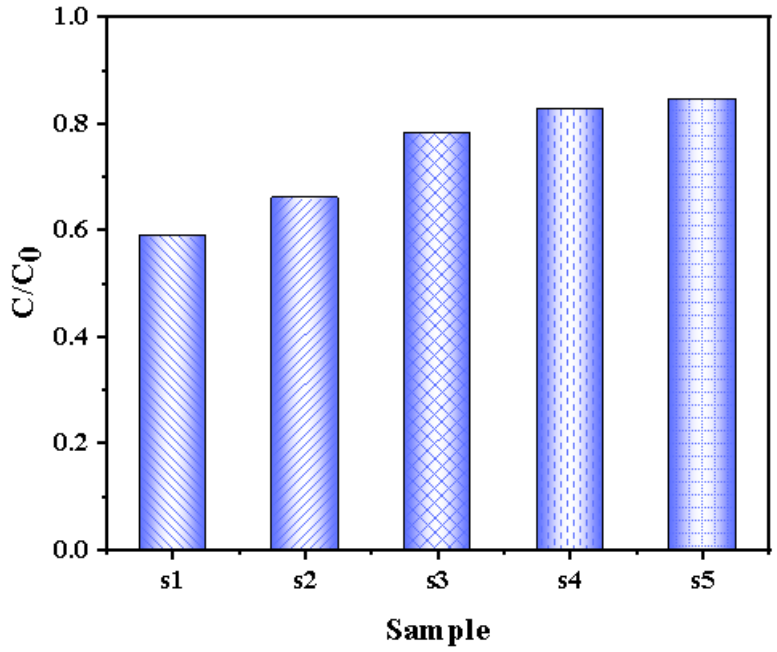

Figure 3.10. Adsorption performance experiments of catalysts: (s1) 350℃; (s2) 450℃; (s3) 550℃; (s4) 650℃; (s5) 750℃.

4. Conclusions

This chapter investigates the photocatalytic degradation performance of nickel-doped three-dimensional (3D) networked TiO_2 nanotube films prepared on the surface of porous titanium, and discusses various influencing factors. Based on the characterization results of the material's phase structure, micromorphology, and chemical composition, it is confirmed that nickel-doped 3D networked TiO_2 nanotube films were successfully fabricated, with well-formed nanotube structures.

Compared with pure TiO_2, Ni_x-TiO_2 has an increased specific surface area, which can provide more active sites for photocatalytic reactions, thereby enhancing the efficiency of photocatalytic degradation of organic pollutants. Under simulated sunlight irradiation, Ni_x-TiO_2 exhibits excellent photocatalytic performance in MB degradation. Among them, $Ni_{7.5}$-TiO_2 shows particularly remarkable photocatalytic performance, achieving a high MB degradation rate of 98.353% within 3 hours under simulated sunlight. After 5 cycles of MB photocatalytic degradation tests, no obvious changes were observed in the photocatalytic activity or crystal structure of $Ni_{7.5}$-TiO_2, indicating its excellent cyclic performance and stability. Compared with the pure titanium sheet substrate, the catalyst prepared using porous titanium as the substrate shows a significant improvement in adsorption capacity. In addition, nickel doping also partially enhances the adsorption capacity of the catalyst. The calcination temperature has a significant impact on photocatalytic performance, and its influence is mainly reflected in two aspects. First, it affects the micromorphology of the catalyst: as the temperature increases, the nanotube structure is gradually damaged and eventually transformed into nanoparticles, resulting in a decrease in specific surface area. Second, it affects the crystal phase: above 550 ℃, anatase TiO_2 transforms into rutile TiO_2, and anatase TiO_2 possesses superior photocatalytic activity.

 doi:10.20944/preprints202604.1380.v1

Funding: This work was supported by the Natural Science Foundation of Sichuan Province (Grant No. 2025NSFSC2065).

Data Availability Statement: The original contributions presented in this study are included in the article. Further inquiries can be directed to the corresponding author.

References

1. E. J. Lu and J. H. Zou, “Research progress of metal/TiO_2 photocatalysts,” Journal of Ceramics, vol. 45, no. 06, pp. 1083-1097, 2024.
2. R. Y. Sun and X. Y. Zhao, “Preparation and application progress of titanium dioxide photocatalysts,” Contemporary Chemical Industry, vol. 52, no. 01, pp. 202-208, 2023.
3. H. S. Hu and P. H. Zhang, “Preparation of S-scheme TiO_2/C_3N_5 heterojunction photocatalyst and its performance in methylene blue degradation,” China Surfactant Detergent & Cosmetics (in Chinese and English), vol. 55, no. 08, pp. 980-988, 2025.
4. Z. Y. Gao, Y. H. Cen, and C. Y. Zhang, “Preparation of titanium dioxide nanospheres and study on their resonance properties in visible light band,” Journal of Guangzhou University (Natural Science Edition), vol. 24, no. 03, pp. 1-9, 2025.
5. J. Zhang, M. R. Guo, S, et al., “Photocatalytic degradation of tetracycline hydrochloride by Fe/Ni-TiO_2 composite,” Environmental Protection of Chemical Industry, Online in Press, pp. 1-7, 2025.
6. H. J. Zhang, G. D. Zhang, and C. Wang, “Preparation and photocatalytic performance of porous TiO_2/CdS nanomaterials,” Transducer and Microsystem Technologies, vol. 41, no. 12, pp. 14-18, 2022.
7. J. P. Wei, Y. L. Ge, et al., “Preparation of two-dimensional anatase/rutile composite and its photocatalytic performance,” Chemical Engineer, vol. 39, no. 04, pp. 14-18, 2025.
8. D. Z. Wang, F. T. Liu, L, et al., “Preparation of porous nano-titanium dioxide thin films and their photocatalytic activity,” Journal of Ceramics, no. 04, pp. 397-401, 2006.
9. X. Chen, L. Y. Wang, et al., “Preparation of anatase-rutile mixed crystal TiO_2 nanofibers and their photocatalytic performance,” Journal of Jilin Jianzhu University, vol. 38, no. 03, pp. 57-62, 2021.
10. JIANG B. F., "Study on photocatalytic treatment of dye-containing wastewater by supported modified nano-TiO_2," [Dissertation], Harbin Inst. Technol., Harbin, China, 2010.
11. DAI J. W., YANG J. Y., GAO X., et al., "Preparation and performance of zinc-doped titanium dioxide photocatalytic antibacterial films," Mod. Transp. Metall. Mater., vol. 5, no. 6, pp. 12–18, 49, 2025.
12. LOU F. P., "Preparation, characterization and photocatalytic performance of nano-titanium dioxide," [Dissertation], Zhejiang Univ. Technol., Hangzhou, China, 2015.
13. ZHANG J., GUO M. R., WANG S. Q., et al., "Photocatalytic degradation of tetracycline hydrochloride by Fe/Ni-TiO_2 composites," Environ. Prot. Chem. Ind., vol. 45, no. 6, pp. 876–881, 2025.
14. LI P. Y., "Preparation and adsorption-degradation performance of carbon/titanium dioxide composites," [Dissertation], Henan Normal Univ., Xinxiang, China, 2017.
15. YU C. Y., WANG B., SONG T., "Research progress in photocatalytic treatment of organic wastewater," Liaoning Chem. Ind., vol. 54, no. 9, pp. 1568–1571, 2025.
16. LI P. Y., "Preparation and adsorption-degradation performance of carbon/titanium dioxide composites," [Dissertation], Henan Normal Univ., Xinxiang, China, 2017.
17. ZHENG X., "Research on the application of photocatalytic technology in sewage treatment," Chem. Eng. Equip., no. 7, pp. 173–175, 2025.
18. WU Z., "Preparation and performance study of titanium dioxide photocatalytic functional materials," [Dissertation], Nanjing Univ. Sci. Technol., Nanjing, China, 2018.
19. WEI F., DING H., LI H., et al., "Preparation of TiO_2 self-cleaning antibacterial glaze by low-temperature secondary firing method," China Ceramics, vol. 61, no. 7, pp. 64–69, 2025.
20. XIANG W. J., ZHU C. J., LIU D., et al., "Photocatalytic degradation of nitrogen oxides by titanocene dichloride under visible light," Appl. Chem. Ind., vol. 48, no. 9, pp. 2153–2155, 2019.
21. HE X. W., ZHOU S. R., LI G. Z., et al., "Preparation and photocatalytic study of rare earth praseodymium and gadolinium ions doped modified nano-TiO_2," J. Funct. Mater., vol. 56, no. 5, pp. 5135–5142, 5166, 2025.

 doi:10.20944/preprints202604.1380.v1

22. WANG Z. G., WEI J. J., WANG H. C., "Application progress of titanium dioxide photocatalysis technology in water quality treatment," Guangzhou Chem. Ind., vol. 48, no. 6, pp. 27–29, 32, 2020.
23. SHANG Z. H., LYU M. Z., LI X. Y., et al., "Preparation and application of different photothermal and photocatalytic nanofiber membranes," Knitting Ind., no. 2, pp. 44–47, 2025 .
24. LIU Q. H., LI K. J., WU S. H., et al., "Degradation of dye wastewater by nano-porous titanium dioxide microspheres photocatalyst," J. Qingdao Univ. Sci. Technol. (Nat. Sci. Ed.), vol. 42, no. 1, pp. 72–77, 2021.
25. HOU B. S., ZENG J. T., LU L. Y., et al., "Research progress of modified TiO_2 photocatalytic degradation of organic dyes," Contemp. Chem. Res., no. 23, pp. 16–18, 2024.
26. LYU M. Z., LIU L. W., LIU Z. Q., et al., "Preparation and photocatalytic performance of FePc/TiO_2 loaded nanofiber membranes," Knitting Ind., no. 3, pp. 58–61, 2021.
27. ZHANG J. R., MA Z. S., HE S. H., "Research progress on preparation and modification of nano-TiO_2 photocatalyst materials," Dyeing Finishing, vol. 50, no. 11, pp. 70–75, 79, 2024.
28. ZHANG Y. F., "Preparation of TiO_2-based nano-composite photocatalysts and their photodegradation performance on dyes," [Dissertation], Soochow Univ., Suzhou, China, 2021.
29. PENG H. K., ZHANG M., YAO N., et al., "Research progress of photocatalytic treatment of microplastics in water environment," Appl. Chem. Ind., vol. 53, no. 10, pp. 2479–2483, 2024.
30. LIU Y., XU H. L., WANG X. Q., "Research progress on preparation and application of TiO_2 photocatalysts," Contemp. Chem. Ind., vol. 50, no. 9, pp. 2217–2220, 2021.
31. YANG J., CHEN X., LIU C. H., et al., "Development and application of photocatalytic technology in energy and environment," Solar Energy, no. 7, pp. 50–61, 2024.
32. WANG J. Z., AO Q. B., JING P., et al., "Preparation and application of porous titanium," Rare Met. Mater. Eng., vol. 51, no. 5, pp. 1907–1918, 2022.
33. WANG H. O., YE F., LIAO C. Z., et al., "Open comprehensive teaching design and practice of titanium dioxide doping modification and its application in photocatalytic degradation of water pollution," Guangdong Chem. Ind., vol. 51, no. 8, pp. 146–149, 145, 2024.
34. LI C. W., YANG Y. F., TAO S. P., "Effect of sintering process on microstructure and properties of porous titanium-based alloys," World Nonferrous Met., no. 9, pp. 1–3, 2023.
35. LI L. R., YANG X. Z., DENG Z. W., et al., "Rare earth modified photocatalytic hydrogen production pathway under the 'double carbon' goal," Oil Gas New Energy, vol. 36, no. 1, pp. 59–65, 2024.
36. DU R. C., LI Y., WANG T., et al., "Research progress on modification of nano-TiO_2 photocatalysts," Chem. Bull., vol. 86, no. 10, pp. 1172–1180, 2023.
37. ZHOU Y., YE L. J., "Preparation of Nd^{3+}-doped TiO_2/rGO and its photocatalytic performance," Chem. Technol. Dev., vol. 53, Suppl. 1, pp. 17–25, 2024 .
38. XIE H. Y., MA C. W., SUN Z. G., et al., "Preparation of polycrystalline nano-titanium dioxide by flame chemical vapor deposition and its application in gas purification," J. Shanghai Polytech. Univ., vol. 31, no. 1, pp. 18–31, 2014.
39. WU D. K., LEI K., SUN H. P., "Characteristics of Pt-doped TiO_2 photocatalysts and their effects on photocatalytic hydrogen production performance," Adhesion, vol. 52, no. 11, pp. 18–21, 2025.
40. HUANG R. Y., "Preparation and photocatalytic performance of titanium dioxide-based photocatalysts," [Dissertation], Jiangxi Univ. Sci. Technol., Ganzhou, China, 2016.
41. WANG S. Z., "Synthesis and performance study of titanium nanotubes," Environ. Sci. Guide, vol. 44, no. 5, pp. 58–61, 2025 (in Chinese). doi: 10.13623/j.cnki.hkdk.2025.05.004.
42. JIANG Z., "Synthesis and activity study of titanium-containing photocatalysts," [Dissertation], Wuhan Univ., Wuhan, China, 2017).
43. HAN L. H., GUO J. Y., MA Q. H., et al., "Research progress in modified nano-TiO_2 photocatalysts for dye degradation," Liaoning Chem. Ind., vol. 54, no. 8, pp. 1412–1416, 2025.
44. WANG J. G., "Construction and catalytic performance of high-efficiency photocatalysts," in Proc. 11th Natl. Conf. Environ. Catal. Environ. Mater., Shanghai Univ. Eng. Sci., Shanghai, China, 2018, p. 130.
45. LIN Y. J., QIAO P., LI X. R., et al., "Heterostructure construction strategies and application research progress of TiO_2 nano-photocatalysts," Chem. Ind. Eng. Prog., vol. 44, Suppl. 1, pp. 159–177, 2025.

 doi:10.20944/preprints202604.1380.v1

46. ZHANG T., YAN X. Y., YUAN H. F., et al., "Research progress of titanium dioxide photocatalysts," Shanxi Chem. Ind., vol. 38, no. 5, pp. 40–42, 2018.
47. HUANG R. F., "Preparation of water-soluble titanium citrate-based photocatalysts and their quasi-homogeneous photocatalytic performance," [Dissertation], Henan Univ. Technol., Zhengzhou, China, 2025.
48. MA Y., ZHENG Q., "Research progress of metal-doped nano-titanium dioxide photocatalysts," J. Yulin Univ., vol. 30, no. 2, pp. 50–55, 2020.
49. QIAO Y. J., SUN J., LI J., et al., "Preparation and characterization of nano-titanium dioxide photocatalysts," Henan Build. Mater., no. 5, pp. 35–36, 39, 2020.